JTTEE5
DOI: 10.1007/s11666-016-0427-3
1059-9630/$19.00 © ASM International

Effect of Spray Particle Velocity on Cavitation Erosion Resistance Characteristics of HVOF and HVAF Processed 86WC-10Co4Cr Hydro Turbine Coatings

R.K. Kumar, M. Kamaraj, S. Seetharamu, T. Pramod, and P. Sampathkumaran

(Submitted October 4, 2015; in revised form May 22, 2016)

The hydro plants utilizing silt-laden water for power generation suffer from severe metal wastage due to particle-induced erosion and cavitation. High-velocity oxy-fuel process (HVOF)-based coatings is widely applied to improve the erosion life. The process parameters such as particle velocity, size, powder feed rate, temperature, affect their mechanical properties. The high-velocity air fuel (HVAF) technology, with higher particle velocities and lower spray temperatures, gives dense and substantially nonoxidized coating. In the present study, the cavitation resistance of 86WC-10Co4Cr-type HVOF coating processed at 680 m/s spray particle velocity was compared with HVAF coatings made at 895, 960, and 1010 m/s. The properties such as porosity, hardness, indentation toughness, and cavitation resistance were investigated. The surface damage morphology has been analyzed in SEM. The cohesion between different layers has been examined qualitatively through scratch depth measurements across the cross section. The HVAF coatings have shown a lower porosity, higher hardness, and superior cavitation resistance. Delamination, extensive cracking of the matrix interface, and detachment of the WC grains were observed in HVOF coating. The rate of metal loss is low in HVAF coatings implying that process parameters play a vital role in achieving improved cavitation resistance.

Keywords cavitation erosion, HVOF/HVAF coating, porosity, surface topography

1. Introduction

The components of hydro plants utilizing silt-laden water for power generation suffer from severe metal wastage due to high-velocity particle impact erosion as well as the flow-induced cavitation. Most of the service-induced failures are attributed to the synergistic effect of both cavitation and silt-assisted erosion (Ref 1-4). The mechanism of material damage during cavitation is mainly attributed to the implosion of high-velocity bubbles onto the component surface, leading to a local increase in stresses in excess of the yield strength of the material. The phenomenon of cavitation erosion gets aggravated under high-turbulent conditions of fluid flow containing the suspended particles (Ref 5-7). The particles encountered in hydro turbine mainly are of quartz, having a hardness value of seven in Mhos scale. The potential of WC-based thermal spray hard coatings of type WC-Co processed through high-velocity oxy-fuel process (HVOF) has been exploited for a variety of engineering applications in view of its excellent abrasive wear resistance. The addition of small amount of Cr increases the corrosion resistance of these coatings, which is considered essential in addition to erosion resistance for hydro plant applications. The erosion performance of these coatings is readily affected by the feedstock powder properties and spray process conditions. The HVOF coatings with nominal composition WC-10wt.%Co-4wt.%Cr are widely adopted in hydro plant components to achieve improved service life. The importance of controlling the porosity, hardness, and toughness properties for achieving improved cavitation resistance properties of these coatings is well reported (Ref 8-11). The coating composition is standardized with the ratio of cobalt to chromium 2:1 by volume and the nominal carbon content is 5.27% for optimum performance (Ref 12-15). The heating of particles in the spray gun system prior to the deposition process would lead to the partial dissolution of WC into the CoCr matrix, and thus controlling the particle temperature and acceleration velocity is considered critical in this type of coating. The resulting coating microstructure would consist of WC, the η phase $(CoCr)_6W_6C$, and a (Co, Cr, W) alloy binder. The high-velocity air fuel (HVAF) technology-based coatings,

R.K. Kumar, S. Seetharamu, T. Pramod and **P. Sampathkumaran**, Central Power Research Institute, Bangalore, India; and **M. Kamaraj**, Indian Institute of Technology, Madras, Chennai, India. Contact e-mails: rkkumarcpri@gmail.com and kamaraj@iitm.ac.in.

Published online: 16 June 2016

which is an advancement over that of HVOF process, utilizes air-fuel mix combustion rather than oxygen-fuel mix, provides higher particle velocities coupled with lower spray temperatures. The spray particles get heated up to a relatively higher temperature in HVOF, leading to a high degree of decarburization which gives rise to the formation of W_2C phases, which increases the embrittlement of coating and reduces the erosion resistance. The occurrence of brittle phases such as W_2C in the coating due to decarburization and increased porosity due to oxidation phenomena needs to be controlled for achieving superior performance of these coatings. Presently, the runner blades made of martensitic stainless steel is widely used and are subjected to a predominantly cavitation phenomenon during the service. The potential of HVAF technology in terms of superior abrasion and slurry wear resistance has been reported recently (Ref 16-21). While the effect of particle velocity, fuel/oxygen ratio, WC grain size, etc., on the performance of coatings processed through different HVOF systems has been studied extensively (Ref 22-25). The effect of the process parameters in HVAF process like particle velocity is not widely reported. The application of hard coatings on to critical runner components, which are subjected to cavitation conditions during service, is being attempted successfully in recent times through design modifications and thus, evaluation of cavitation resistance becomes very important for these coatings.

2. Experimental Program

2.1 Materials and Coating Preparation

The reference 86WC-10Cr-4Co-type HVOF coating of 410 μm thickness was made onto SS410 grade stainless steel substrate material, at a spray particle velocity of 680 m/s, using JP5000 system. The substrate material was surface-cleaned by grit blasting using 24 grit Al_2O_3 at 60 PSI pressure and preheated to 90 °C prior to the HVOF coating deposition. Three types of HVAF coatings processed at particle velocities of 1010, 960, and 895 m/s were made using AK06 HVAF gun with three different nozzles of 5O, 5E, and 5L, for comparison. The different velocities were achieved through different degrees of expansion nozzles used for thermal spraying. The mean particle velocity and temperature were measured using the AccuraSpray-G3C sensor system of Tecnar, Canada. The substrate was preheated to 105–115 °C, before spraying. The sintered and agglomerated type spray powder of ~1.2 μm carbide grain was used in both the coating process. The coating morphology, porosity, and hardness were evaluated on the cross section of the coating. The indentation toughness was measured at a test load of 10 kg on the cross section of coatings using the toughness equation developed by Niihara (Ref 26). The cavitation erosion resistance was evaluated using a vibratory type cavitation test rig for a maximum duration of 13 h. The

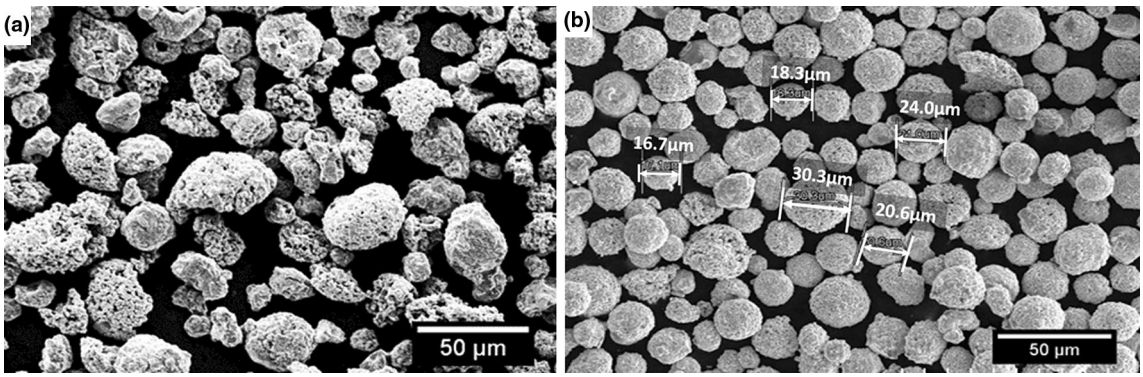

Fig. 1 Morphology of feedstock powder 86WC-10Co-4Cr used for (a) HVOF and (b) HVAF coatings

Table 1 Spray parameters used during the coating processes

JP5000 HVOF		AK06 HVAF			
Powder: Praxair 1350VMAgglomerated and sinteredSize: −45 to +16 μm		Powder: Amperit 558.059 HC StarckAgglomerated and sintered−45 to +20μm			
Oxygen flow@210 PSIG, SCFH	1850	Air, PSIG			90.3
Kerosene @170PSIG, SCFH	5.8	Propane, PSIG			83.8
Carrier gas flow (N_2) @ 50 PSIG, SCFH	23	Carrier gas flow (N_2) @ 140 PSIG, SLPM			21
		H_2 injections @ 140 PSIG, SLPM			20
Stand-off distance, inch	15	Stand-off distance, inch			7
Powder feed rate, g/min	90	Powder feed rate, g/min			133
Deposit thickness per pass, μm	15	Deposit thickness per pass, μm			28
Particle velocity, m/s	680*	Particle velocity, m/s	Nozzle 5O	Nozzle 5E	Nozzle 5L
			1010 +/−4	960 +/−3	895 +/−2

* provided by coating supplier

diamond spray-polished coating specimen of size $15 \times 15 \times 7$ mm^3 was used for the test. The cavitation resistance in terms of mass loss of coating was measured after every 1 h. The progress of the surface damage morphology of the coatings was observed in Scanning Electron Microscope. The homogeneity of the cohesion between different layers has been examined qualitatively through measurement of scratch depth across the cross section, carried out using Nano indenter G200, Agilent Technologies, USA. The morphology of the spray powder used is shown in Fig. 1, and the spray parameters adopted for HVOF and HVAF coatings are given in Table 1. The cross section of the coatings prepared is shown in Fig. 2. The measured coating thicknesses were in the range of 380-420 μm.

2.2 Characterization of Coatings

The coated specimens were cold-mounted in an epoxy polished using 220, 500, and 1200 grit diamond disks with water as the lubricant. The final polishing was done using 9, 3, and 1 μm diamond spray solutions, sequentially. The surface roughness of both as-sprayed coating as well as the polished samples was measured using Taylor Hobson SURTRONIC-25 tester. The coating specimen was secured on a flat granite base table, and the stylus of the pickup spindle was adjusted to horizontal. The cut-off and evaluation lengths are chosen as 0.2 and 4 mm, and measurements were taken at the center of the coating specimen. The average of four readings was reported. While, the as-sprayed coatings had an average roughness Ra, 2.28 to 4.48 μm, the polished coatings had the Ra value less than 0.2 μm.

2.2.1 Phase Composition. The phase composition analysis of coatings and the feedstock powders was analyzed using PANalytical x'pert'pro diffractometer with Cu-Kα radiation in the $30° \leq 2\theta \leq 90°$. The integral intensities of WC and W_2C were assessed corresponding to (100) and (101) peak, respectively.

2.2.2 Mechanical Properties. The microhardness of the coatings was measured on the polished cross section using Zwick30 hardness tester at a test load of 300 g. The porosity of coatings was measured on the polished cross section of the coatings by image analysis at 100X using ZEISS Axioimager200 microscope. Both hardness and porosity readings were reported as the average of seven readings. The Young's modulus of the coatings was measured using nanoindentation tester of Agilent Technologies G200 at a test load of 400 mN for all the coatings. The indentation toughness of coatings was measured based on the crack length that appeared under the test load of 10 kg, on the cross section, using INSTRON WOLPERT930 tester, and the fracture toughness was calculated according to Niihara equation for radial Palmqvist crack regime (Ref 26). The indentation edge cracks par-

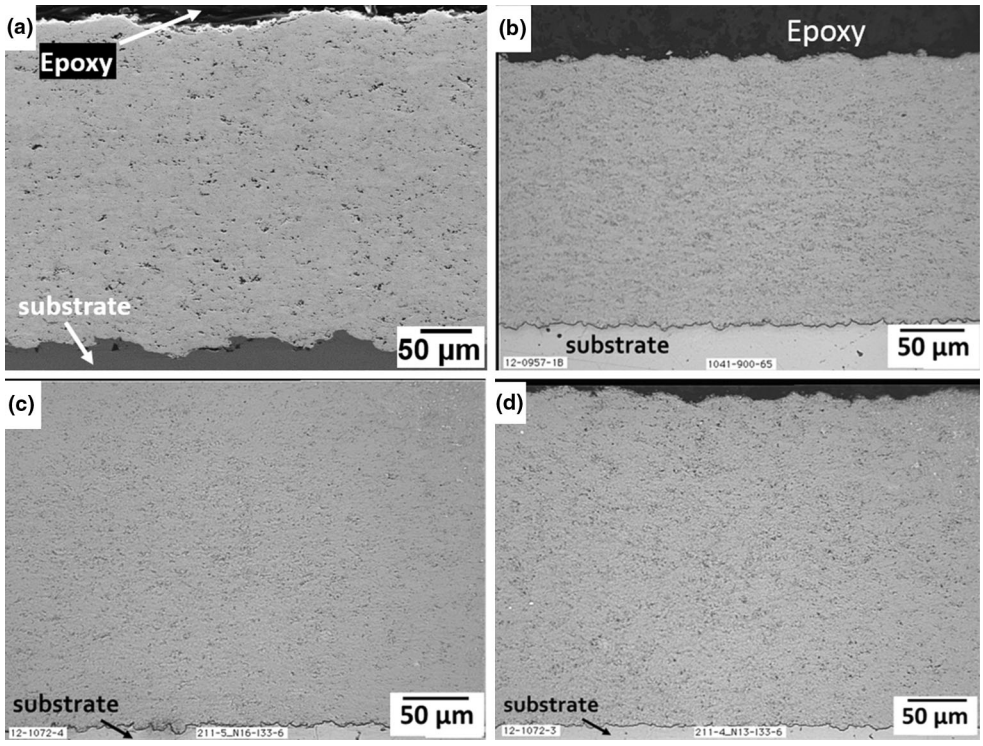

Fig. 2 SEM image of the coatings HVOF (a), AF1 (b), AF2 (c), and AF3 (d)

allel to the substrate were only considered for the crack length measurements.

2.2.3 Residual Stress Measurements. The residual stress on the diamond polished coating surface was measured using a Rigaku stress analyzer of model STRAINFLEX MSF-2M. Cobalt radiation was chosen to obtain the best resolution of x-ray diffraction peaks. The average of three readings was reported. The residual stresses were measured using the standard $\delta 2\theta$ versus $\mathrm{Sin}^2\ \psi$ method described elsewhere (Ref 27). The (121) diffraction plane with a peak at 2θ at 166.2 deg was measured. The stress coefficient was used to calculate residual stresses from peak positions. The minimum elastic modulus values of 312 and 253 GPa obtained during nano indentation of HVAF and HVOF coatings, respectively, were used for the stress calculation. The value of Poisson ratio of 0.18 was assumed for all the coatings studied.

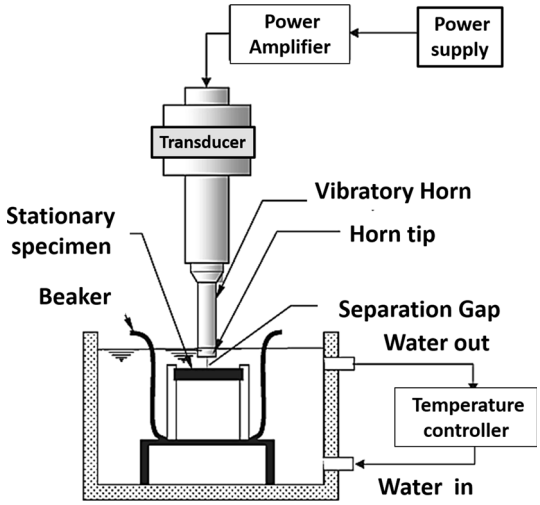

Fig. 3 Vibratory cavitation erosion test setup used

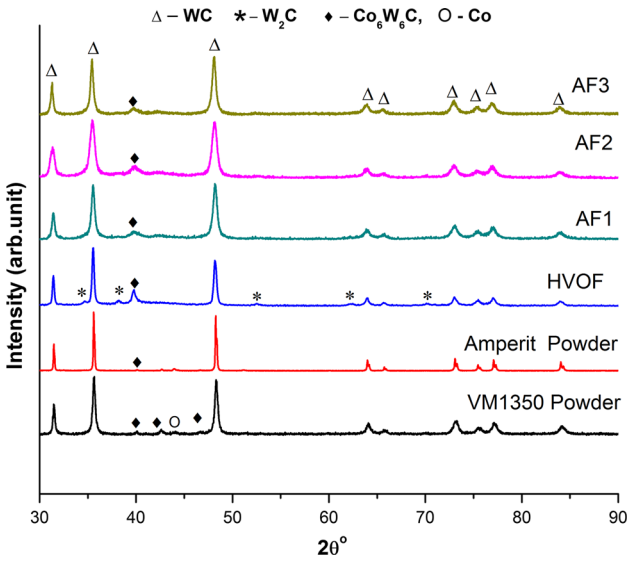

Fig. 4 XRD spectra of the powder material used for HVOF and HVAF coatings

2.2.4 Cavitation Erosion Resistance. The cavitation erosion tests were conducted using a commercial ultrasonic processor (VCX 1500, Sonics & Materials, USA) as per the guidelines of ASTM G32-03. While the vibration frequency of 20 KHz was used as per the standard, the peak-to-peak amplitude was chosen as 100 μm instead of 50 μm. The literature report on international cavitation erosion test (ICET) covered wider diversity in vibration amplitudes in the range of 28-117 μm in the basic operating parameters, and the cavitation test conditions followed in the present study conform to the published information elsewhere (Ref 28, 29). The results in terms of relative cavitation erosion of the hard resistance of hard coatings under identical test conditions were reported.

The vibratory cavitation test setup used is shown in Fig. 3. Tap water was used as the solution. The diamond-polished test specimen of size 15 × 15 mm^2 was secured below the oscillating horn tip with a gap of 1 mm. The specimen was exposed to predetermined time intervals and the weight loss was recorded after cleaning the sample ultrasonically with acetone. The mass loss of the specimen was recorded after every 1 h using an analytical balance (METTLER 200) with 0.1 mg resolution. Multiple specimens were used for varied exposure tests. The tests were continued up to a maximum of 13 h till steady rate of erosion loss was achieved. The initial test was carried out for 30 min duration, keeping in view the possibility of measurement of weight loss in the analytical balance used.

2.2.5 Scratch Resistance Measurements. The qualitative interlayer cohesive properties of both HVOF and HVAF coatings were attempted through scratch testing on the cross section, in a Nano Indenter equipment (G200 Agilent Technologies, USA). The maximum load of 200 mN and the scratch velocity of 10 μm/s were used during the test. During the ramp-load scratch test, the Berkovich indenter tip was brought into contact with the sample; then, the tip is loaded at a constant loading rate while simultaneously translating the sample. Prior to and following the scratch test, a single-line-scan of the surface topography is completed for comparing the original sur-

Table 2 Mechanical properties of HVOF and HVAF coatings

Coating designation	Spray gun/nozzle	Hardness (HV0.3)	Porosity (%)	Fracture toughness (MPa√m)	As sprayed coating surface roughness (Ra)
HVOF	JP-5000	1180 ± 70	0.98 ± 0.3	3.86 ± 0.7	4.48
AF-1	AK06/5O	1473 ± 40	0.52 ± 0.13	5.6 ± 0.15	2.28
AF-2	AK-06/5E	1380 ± 40	0.46 ± 0.19	6.86 ± 0.8	3.12
AF-3	AK-06/5L	1290 ± 30	0.42 ± 0.16	6.33 ± 0.5	3.41

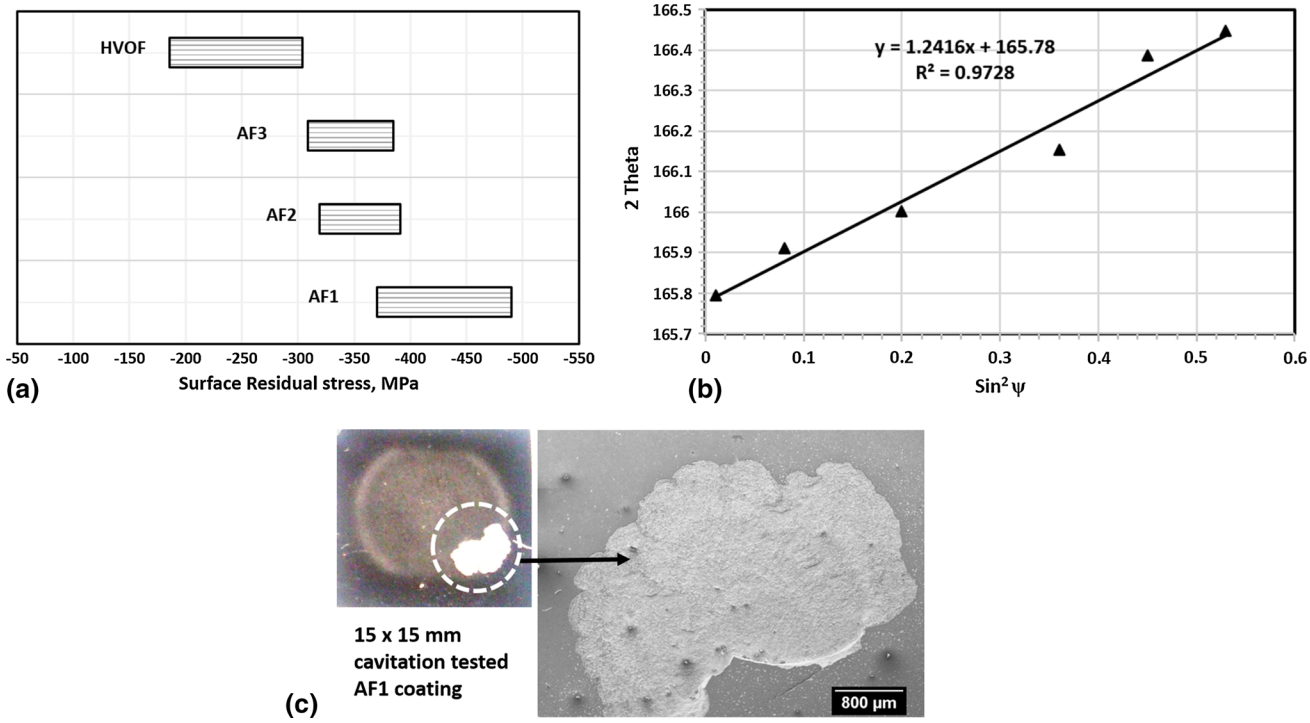

Fig. 5 (a) Residual stress in different coatings. (b) Variation of 2θ vs. $Sin^2\psi$ for AF1 coating during XRD-based stress measurement. (c) Cracking/delamination of AF1 coating at the cavitation damage boundary

face to the deformation caused by the scratch test. The evaluation of deformation mechanisms and the quantification of deformation were carried out from the original and residual single-line scans. The indenter was traversed from the interface to the surface as well as from the surface to the interface, and the scratch depth was monitored during the movement.

2.2.6 Surface Damage Profiles. The evolution of surface damage during cavitation was observed through SEM using Quanta 400 to get insight into the mechanism of damage progression during successive intervals of cavitation. Figures 7 to 9 show the topography of various times varied cavitation-tested coatings.

3. Results and Discussion

3.1 Phase Composition

The morphology of the feedstock powder used in HVAF coatings (Amperit 558.059) has shown comparatively higher spherical in shape than the powder used for the HVOF coating (VM 1350), (Fig. 1). The XRD spectra of both the powders and coatings have shown predominantly WC peaks. The absence of W_2C peak in the VM 1350 feedstock powder and the occurrence of prominent crystalline peaks of W_2C in the HVOF coating imply that decarburization of WC has taken place during the spray process (Fig. 4). However, the incidence of W_2C peak was absent in HVAF coatings. It is widely reported that the formation of η-phase is promoted in HVOF coating during splat quenching and caused by dissolution of WC in the cobalt matrix. The observed η-phase W_6Co_6C peak in all the coatings is commensurate with the findings reported widely (Ref 30).

3.2 Mechanical Properties of Coatings

The results of the hardness, toughness, roughness value, as well as the porosity of the coatings evaluated, are given in Table 2. The microhardness and indentation toughness values of the HVAF coatings were comparatively higher than that of the HVOF coating. The AF1 coating sprayed with the maximum velocity of 1010 m/s has shown the highest hardness value of 1473 HV0.3 and comparable indentation toughness. At moderate spray velocities in the range of 900-960 m/s, minimal change in toughness properties was observed. The minimal variation in the observed hardness value of all the three HVAF coating indicates uniformity in distribution of WC particles in the CoCr matrix compared to that of the HVOF coating. The HVOF coating exhibited increased porosity levels and relatively lower toughness than the HVAF coatings. The observed toughness values of ~4 to 7 MPa√m are consistent with the reported literature on similar WC-based coatings (Ref 31).

3.3 Residual Stresses in Coatings

All the diamond ground-polished coating surface has shown compressive residual stress. The observed com-

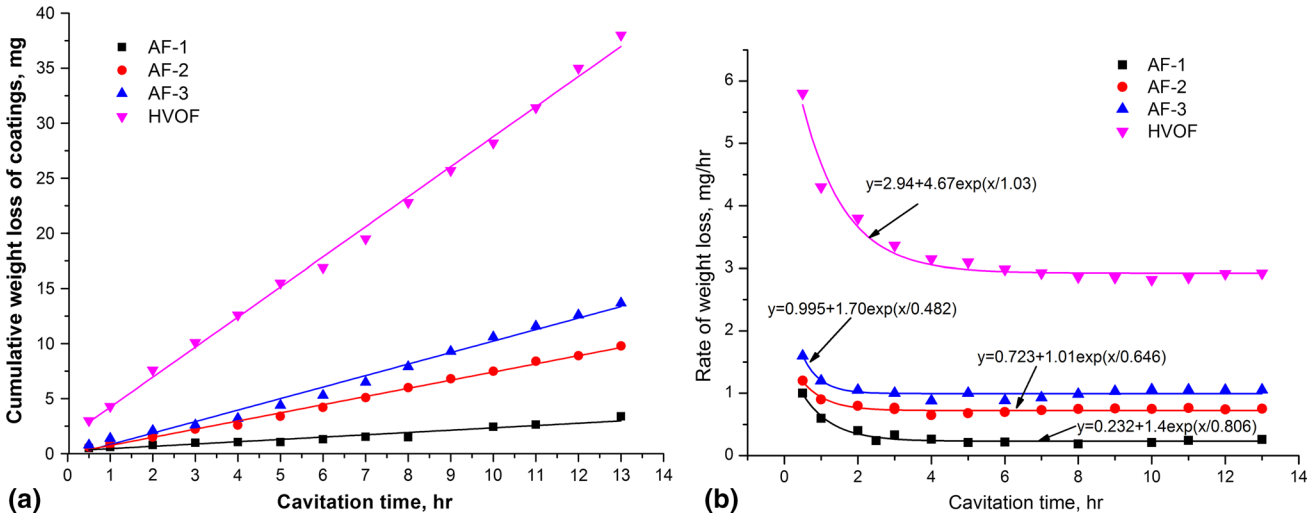

Fig. 6 (a) Cumulative weight loss of different coatings during cavitation. (b) Rate of weight loss of different coatings during cavitation

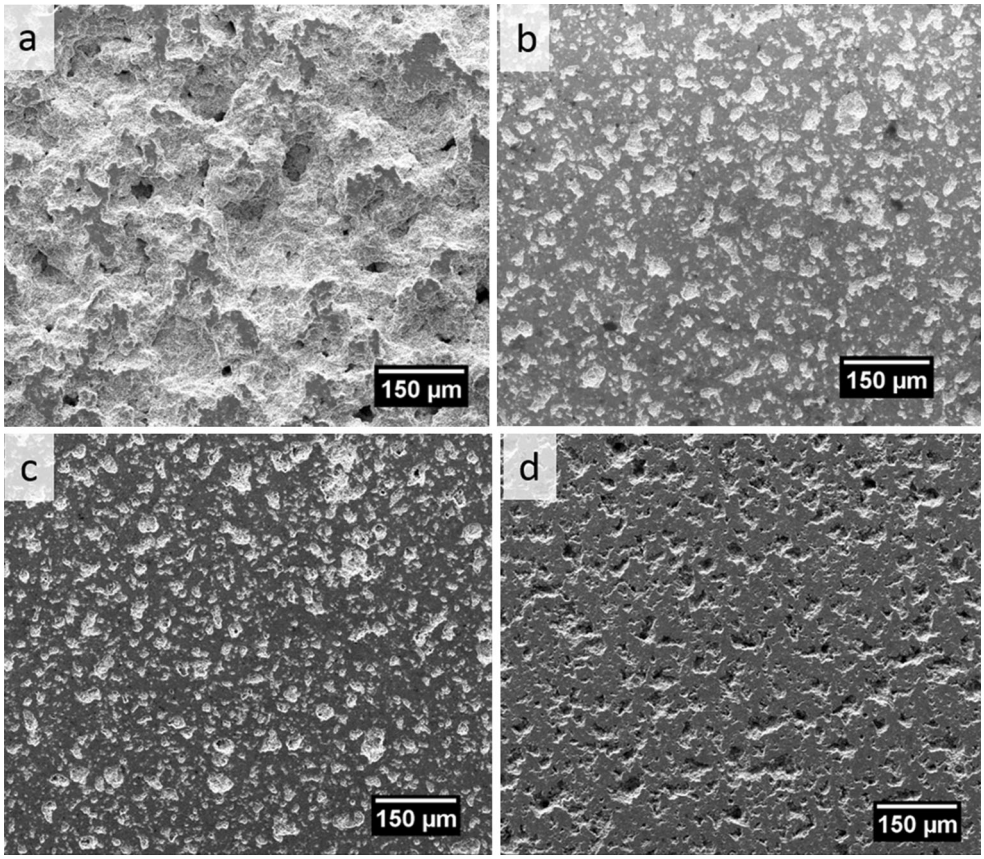

Fig. 7 Surface damages after cavitation exposure of 3 h; HVOF (a), AF1 (b), AF2 (c), and AF3 (d)

pressive state of stress on the surface of diamond ground-coating specimens of both HVOF and HVAF agrees with the findings reported (Ref 32). The stress value on the surface of the coatings increases with increase in spray velocity. Bansal et.al has reported the development of compressive state of surface stresses during the HVOF process and their magnitude is affected by the kinetic energy of the particles (Ref 33, 34). Comparatively lower temperatures and high impact velocity in HVAF over that of HVOF process produce significant peening stresses due

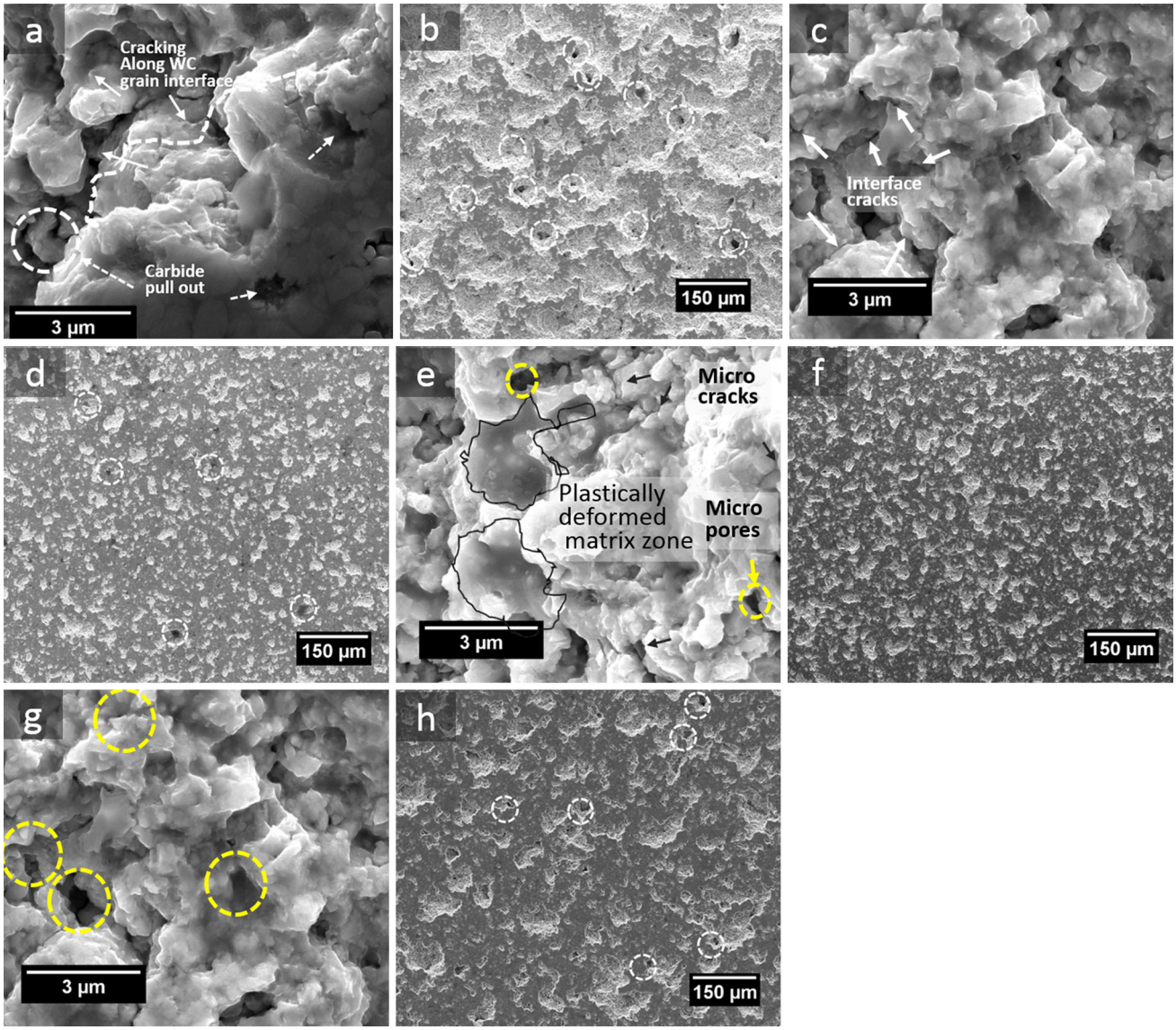

Fig. 8 Surface damage profiles after 1 h cavitation; HVOF (a) and (b), AF1 (c) and (d) , AF2 (e) and (f), and AF3 (g) and (h)

to the kinetic energy of impinging particles with the previously deposited material. While the HVOF coating had shown the compressive stress level of up to 300 MPa, the HVAF coatings have shown compressive stress in the range of 360-500 MPa, indicating the evidence of shot-peening effect on the deposited layers at higher spray velocity, (Fig. 5a). The variation of surface residual stress on the coating at spray velocities in the range of 850-950 m/s is observed to be small. The typical variation of observed 2θ verses Sin^2 ψ during the stress measurement of AF1 coating is shown in Fig. 5b. The incidence of bulging, cracking, and delamination has been observed in the highly stressed AF1 coating after prolonged cavitation exposure indicating that the additional compressive stress introduced by the repeated bubble impact during cavitation increases local stress in excess of fracture strength of the coating (Fig. 5c).

3.4 Cavitation Resistance of the Coatings

The results of the cumulative weight loss of coating with cavitation time as well as the rate of weight loss during cavitation experiments are shown in Fig. 6a, b. All the coating materials undergo metal loss right from the beginning of cavitation exposure and steadily increases with cavitation time. The progressive damage, during the initial period, was observed in terms of increase in the affected area of the initial polished flat surface morphology. The steady rate of metal loss due to cavitation in HVAF coatings was much lower, 0.23-0.99 mg/h, compared to 2.94 mg/h in HVOF coatings. The reduction in

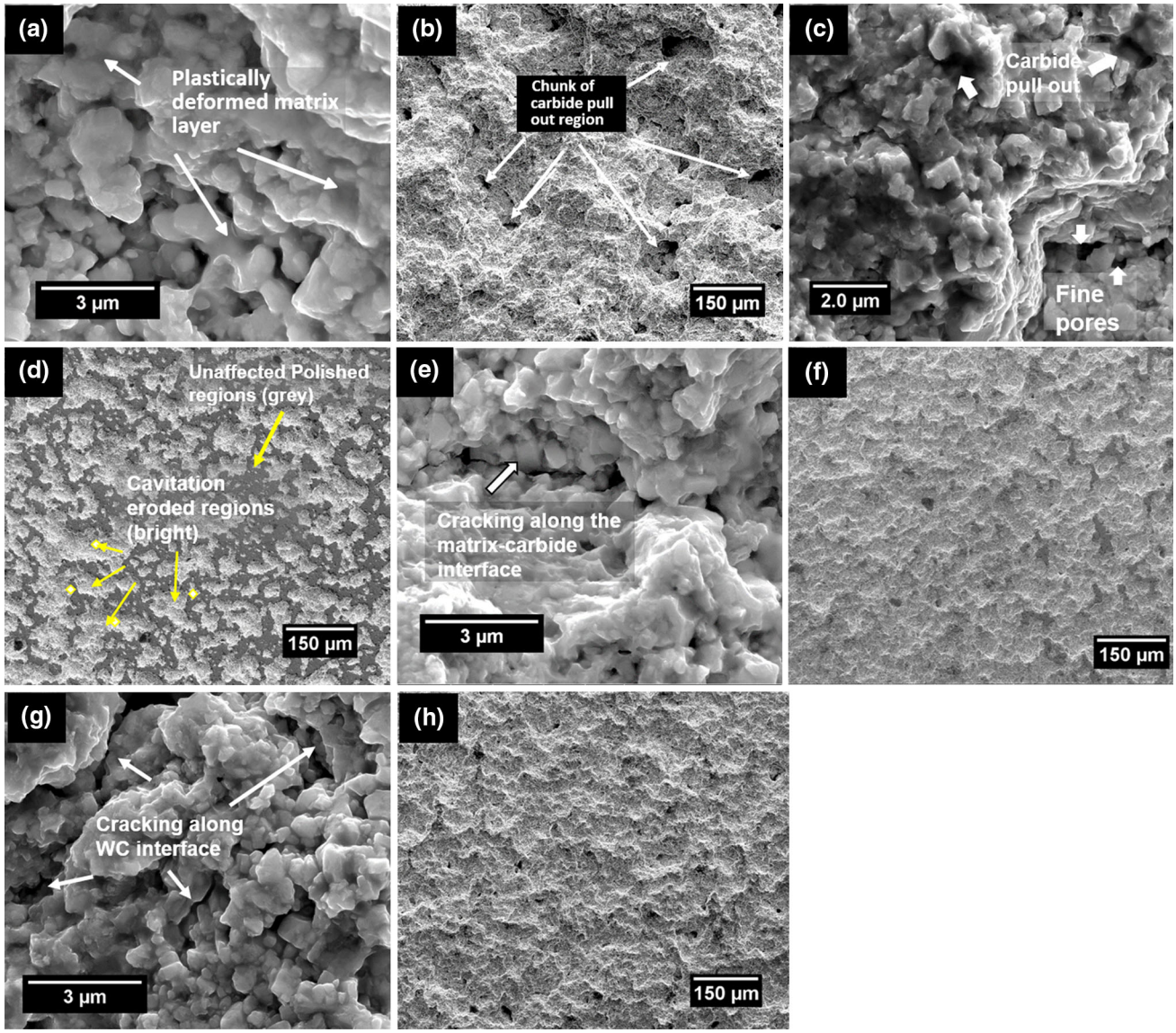

Fig. 9 Surface damage profiles after prolonged cavitation exposure; HVOF-9h (a) and (b), AF1-13h (c) and (d), AF2-13h (e) and (f), and AF3-13h (g) and (h)

mass loss factor of HVAF coatings after 13-h cavitation is in the range of 3.2-3.8 compared to HVOF. The preliminary results of the analysis of the HVAF coatings were reported earlier by the author (Ref 35).

The evolution of surface damage during cavitation was observed through SEM and the surface damage profiles generated after different cavitation intervals are shown in Fig. 7 to 9. The damage appears to get initiated predominantly in the regions of pores and lead to the formation of the crater in the affected areas with cavitation time. The HVOF coating had shown complete loss of original polished flat surface morphology after 3 h of exposure, closely coinciding with the start of a steady rate of metal loss (Fig. 7a). The HVAF coatings exhibited the comparatively lower degree of damage during the initial stages, as observed from the integrity of the polished surface morphology during the same period (Fig. 7b, d). The area percent of the original polished surface, affected after 3 h exposure, was calculated through image analysis and the average of three images was reported. The affected area in case of HVOF coating was 32.1% and the corresponding damage area of 21.2, 22.5, and 25.48% was observed for the AF1, AF2, and AF3 coatings, respectively. The substantial increase in surface damage morphology, as noted on the HVOF coating, after 3-h exposure, corroborates this finding. During the initial cavitation exposure of 1 h, HVAF coatings had shown a minimum reduction in weight loss factor of 2.8 over that of HVOF, under the cavitation test conditions followed in the field.

The surface damage experienced by the coatings, both during the initial and prolonged cavitation exposure period was observed at high magnifications (25000×), and the

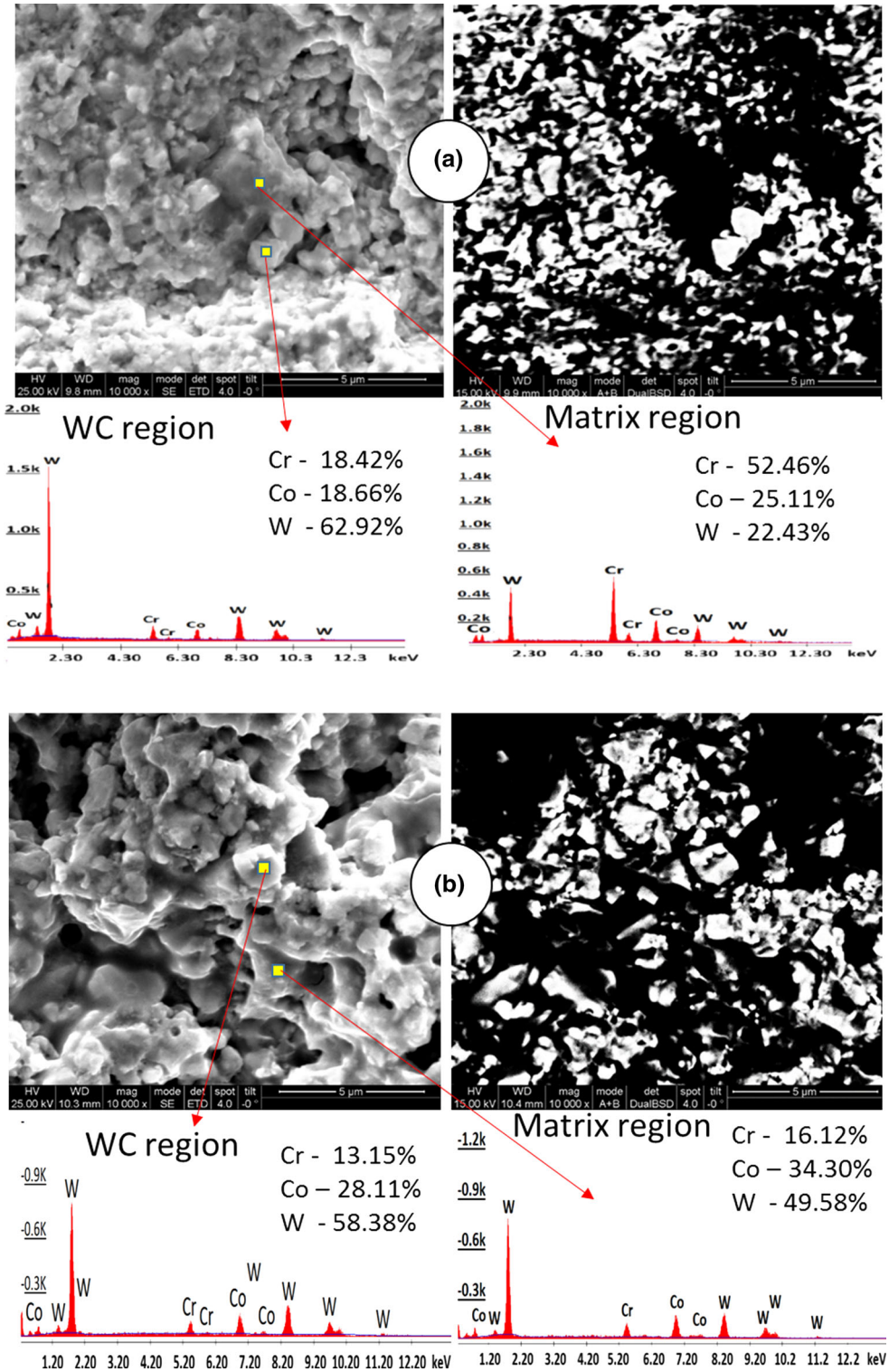

Fig. 10 SE and BSD imaging of cavitation-tested coatings with EDS analysis on the WC and matrix regions (a) AF1-13 h (b) HVOF-9 h

SEM micrographs are shown in Fig. 8 and 9. The HVOF coating exposed for the initial 1-h period has indicated a loss of matrix material with evidence of continuous microcracks extending over several WC grains, in severely affected cavitation regions. Also, dislodgment of carbide grains arising out of complete matrix removal could be seen (Fig. 8a). The cavitation-damaged surface, during the initial period, also revealed the distribution of fine pin

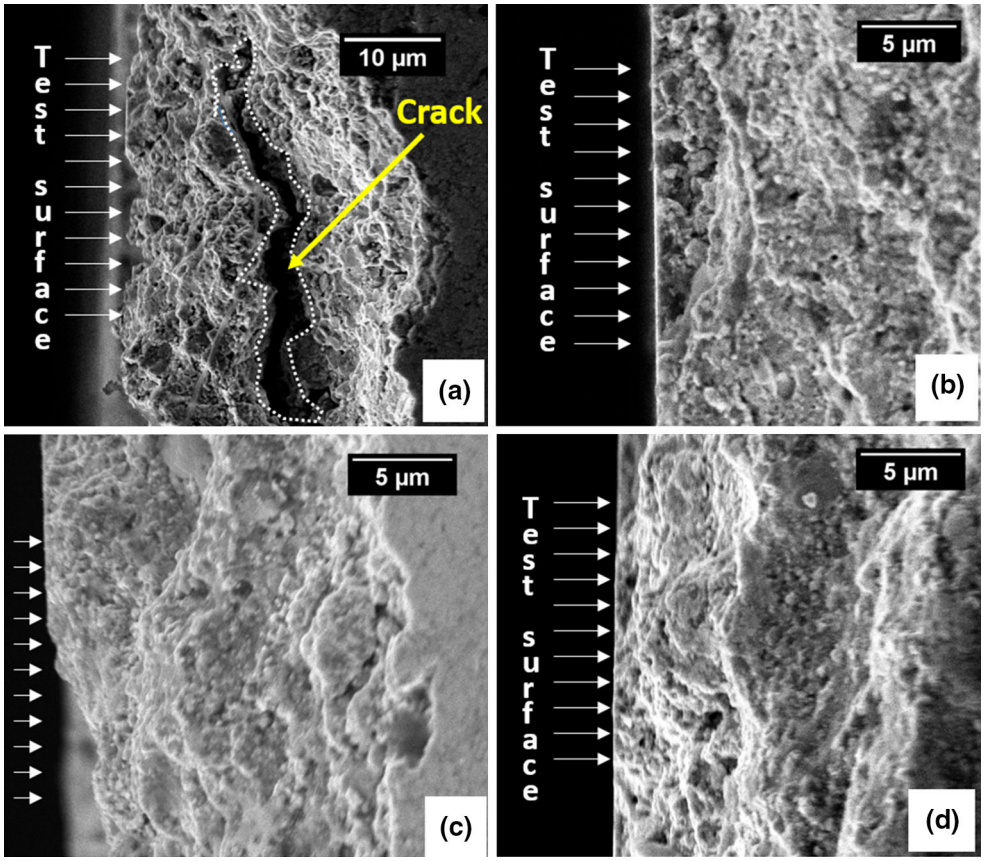

Fig. 11 Sub-surface damage of coatings as observed through the cross-sectional micrographs HVOF (a), AF1 (b), AF2 (c), and AF3 (d)

hole porosities (Fig. 8b) and the damage is observed to get initiated in these regions. The observed porosity/pit-like regions in all the three HVAF coatings are relatively low (Fig. 8d, e, g). In general, the cavitation-damaged surface of HVAF coatings indicated features of the plastically deformed matrix, forming a protective covering and providing reinforcement for the WC grains (Fig. 8c, e, g). The observed interface cracks at random locations are discontinuous in nature and very small in size (<1 μm). The AF3 coating sprayed with marginally higher velocity over that of HVOF coating has shown similar damage morphology with a relatively low degree of plastic deformation in the matrix, and the matrix cracking was insignificant (Fig. 8g). The surface damage observed under high magnifications suggests that the mode of metal removal in the early stages of HVOF coating included cracks along the carbide-matrix interface in combination with carbide dislodging. The extent of cracking in HVAF coatings is minimal at random locations and the coherency of plastically deformed CoCr matrix region could be clearly seen (Fig. 8c, e) during the same period.

The distinctive appearance of protruding WC grains (absence of surrounding matrix) in combination with the complete loss of the original polished area after prolonged exposure (~9 h) of HVOF coating, is suggestive of the lower degree of cohesiveness of the coating (Fig. 9a). The improved coherency of the matrix-carbide interface in HVAF coatings was evidenced from the higher elastic strain energy during the nanoindentation test as well as the effective reinforcement provided by the matrix in holding the WC grains during cavitation. The tenacious quality of the matrix could also be seen through the existence of unaffected original polished regions, even after 13 h of cavitation (Fig. 9d, f, h), with a minimal level of cracking in isolated regions within the cavitated area.

The evidence of matrix undergoing deformation preferentially was ascertained through Backscattered Electron imaging (BSE) of both the matrix region (gray colored) and the WC grain regions (bright) along with compositional analysis by EDS, and the results are shown in Fig. 10. The composition in the matrix region of AF1 coating shows primarily Cr and Co with minor amounts of W content. However, the corresponding region of the HVOF coating is rich in W, Co, and Cr. The prominent W_6Co_6C and W_2C peaks observed in the XRD spectra of HVOF coating (Fig. 4), lend support to this in view.

The sub-surface damage due to cavitation in different coatings was analyzed in the cross-sectional micrographs through SEM. The cavitation-tested specimen was cut by EDM and polished using 9 and 1 μ diamond spray, and the micrographs beneath the tested surface are shown in

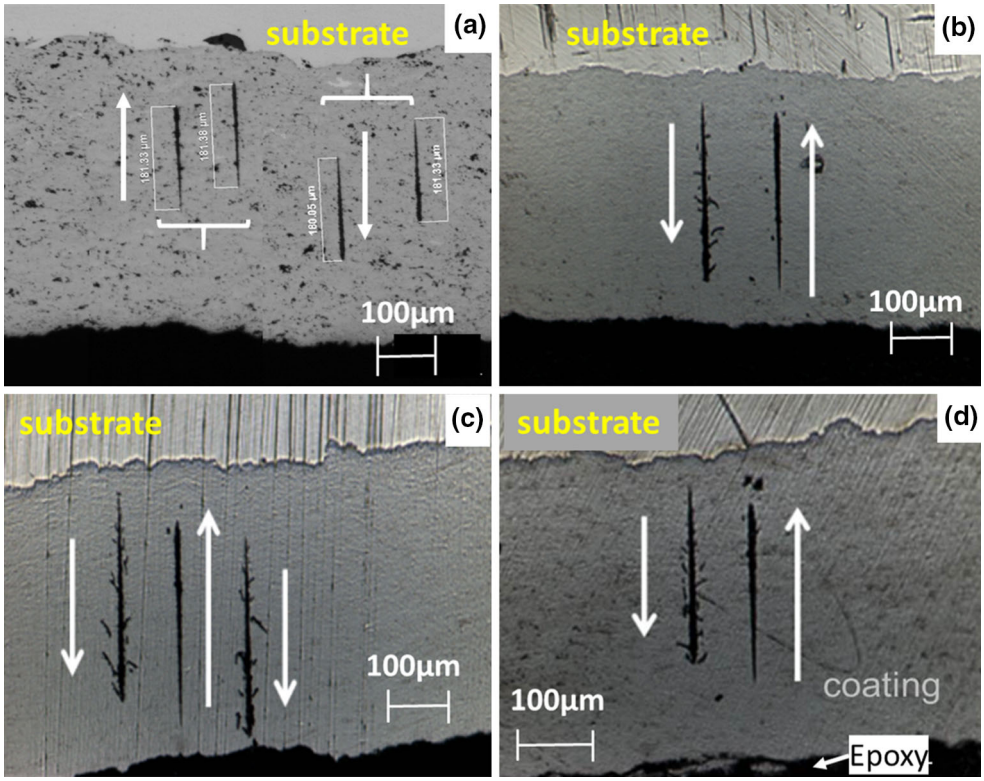

Fig. 12 Scratch profile of HVOF and HVAF coatings HVOF (a), AF1 (b), AF2 (c), and AF3 (d)

Fig. 11. The visibility of cracks parallel to the coating and dislodging of carbide grains was very clearly seen in the HVOF coating (Fig. 11a). The repeated bubble implosion appears to cause the binder matrix to undergo deformation on a continual basis, giving rise to the formation of layered deformed structure. The existence of dimple morphology of the sub-surface layers and macrocracking observed at different locations in the HVOF coating is indicative of the sustained strain condition of the matrix layers and eventual cracking. The extent of strained layers with an indication of degeneration of WC particles in AF1 coating was observed to be quite low and restricted just beneath the tested surface. In the successive region, the layered built-up structure is quite undamaged leaving a comparatively smooth topology. The layered deformation could be more clearly seen in AF2 and AF3 coatings. The prevalence of isolated finer carbide grains, resulting after removal of the binder matrix, could be seen just below the cavitated surface in the case of AF3 coating. The coherency of the built-up layers with minimal cracks in all the three HVAF coatings is suggestive of improved resistance to microcracking during cavitation. The increased toughness of the HVAF coatings lends support to the above points.

Under the conditions of the low cohesive strength of built-up layers as affected by the spray velocity and temperature, the localized bubble implosion pressure causes disintegration of the WC grains from the matrix through the mechanism of microcracking in weak interface regions → networking of cracks → dislodgement of WC grains followed by gross removal of the coating by delamination. The HVOF coating has shown the formation of deep pits with evidence of delamination of the coating layer as well as a complete detachment of the WC grains. The significant reduction in the rate of metal loss as observed in HVAF coatings implies that the porosity and hardness of coating affect the cavitation resistance. The higher particle impaction velocities achieved during the HVAF process increase the cohesive properties of the inter-layers as well as the CoCr matrix-WC interface properties and hence the cavitation resistance.

3.5 Scratch Testing of Coatings

The view of the scratch profile obtained in the cross section of different coatings is shown in Fig. 12. The literature on the evaluation of cohesive properties of thermal spray coatings through scratch testing was reported recently (Ref 36). When the indenter was moved from the interface to the surface (tensile straining of the coating inter-layer), HVAF coatings have shown the characteristics of coating material removal in the direction of the scratch, extending laterally from the edges of the scratch groove. However, the scratch profile was observed to be very smooth without coating material fragments when the indenter is moved from surface to interface (compressive straining of inter-layer). In the case of HVOF coating, the corresponding region is not evident for both tensile and

compressive strain conditions. Thus, the higher impact velocity of spray particles during each layer built up in HVAF coating process, brings-in elastic recovery of the preceding compressed splat layer under the conditions of tensile strain. The scratch depth is nearly the same for both the coating types during the movement interface to the surface. The variation of scratch depth with the load during the movement of the indenter from the surface to the interface for AF1 and HVOF coating is shown in Fig. 13. The HVAF coatings show nearly a uniform increase in depth during both directional movements of the indenter. However, the measured scratch depth is nearly 35% higher in HVOF coating when the indenter was moved from the surface to interface (Fig. 14b), indicating higher plasticity of the coating. Moreover, the load-scratch depth trace is quite uniform for AF1 coating while the HVOF coating depicted a ripple pattern with a number of steps. The calculation of elastic strain recovery during nano-indentation was determined based on the area under the unloading curve. The total deformation energy is considered equal to the area under the loading curve. Four indentations were made on the surface of the coating, and the range of elastic strain energy observed in all coatings is shown in Fig. 15. In general, the observed elastic strain energy was higher in HVAF coatings compared to HVOF coating and that a maximum increase in the elastic recovery of 40.2% was observed at a maximum spray velocity of 1010 m/s. This appears possibly due to the combined effect of increased hardness and surface compressive residual stress in these coatings.

4. Conclusions

The systematic study on the comparative cavitation resistance of both HVOF and HVAF processed tungsten carbide coatings indicated the following.

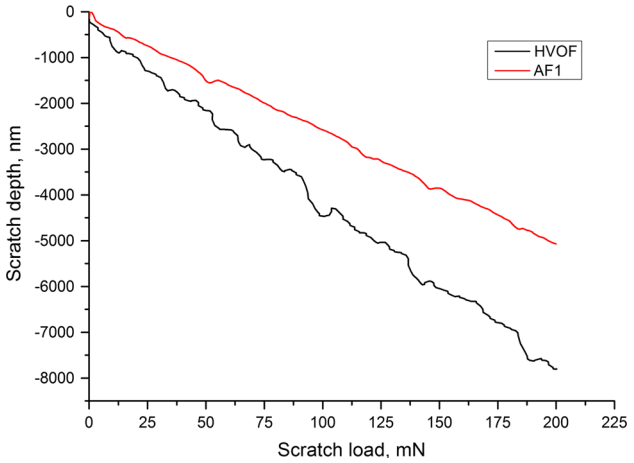

Fig. 13 Scratch load-depth trace obtained during nano-scratch test AF1 (a) and HVOF (b)

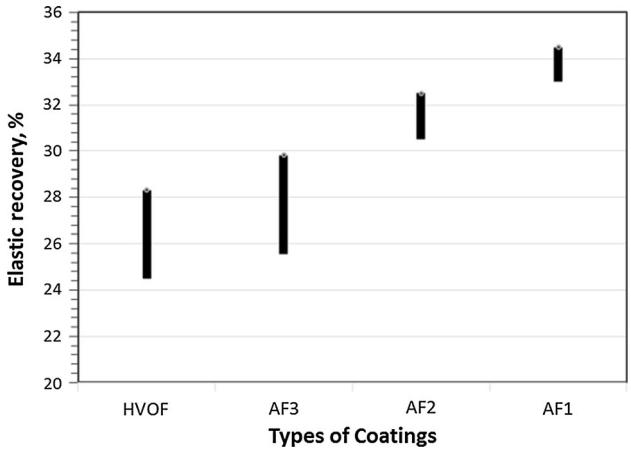

Fig. 15 Percent elastic recovery during nano-indentation of different coatings

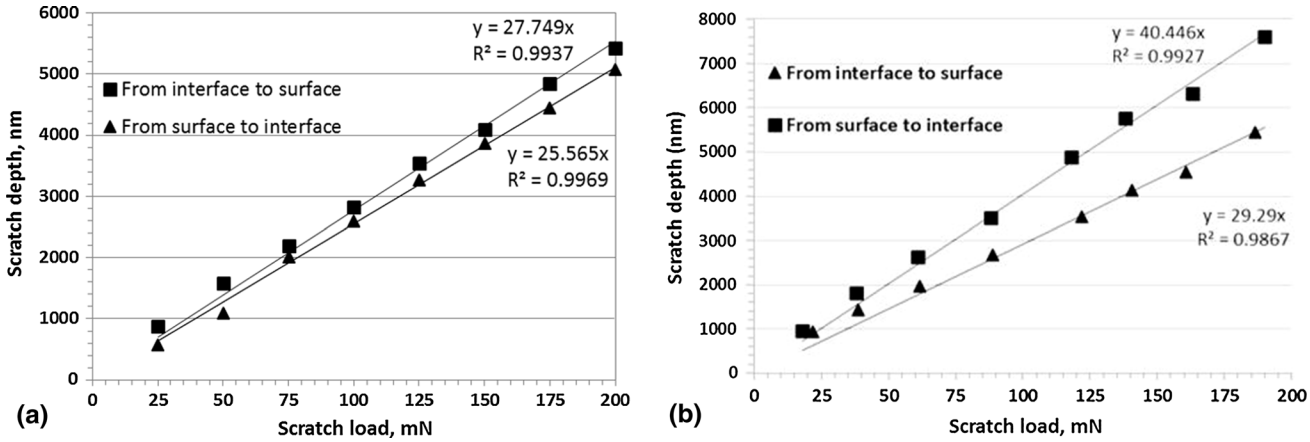

Fig. 14 Variation of depth into the coating surface during scratch loading in two scratch directions AF1 (a) and HVOF (b)

- HVAF coatings exhibit lower porosity levels, higher hardness, toughness, and superior cavitation resistance compared to HVOF coating for the same spray powder conditions. The higher toughness values, as well as the consistency in scratch depth results in HVAF coatings, support these findings.
- The mechanism of metal removal in HVOF coating during cavitation includes microcracking of matrix phase $\rightarrow$ networking of cracks along the boundaries of WC grain interface $\rightarrow$ dislodging of WC grains $\rightarrow$ delamination of the coating.
- HVAF coatings sprayed with higher spray velocities result in improved toughness and cohesiveness of splat layers of the coating that provides better cracking resistance under bubble implosions. The lower degree of surface damage in the initial cavitation period and the progress of damage during cavitation bubble imploding are noticeably affected by the ability of the CoCr matrix's cracking resistance. The superior cavitation resistance property of HVAF coatings was thus attributed to the increased hardness, toughness, and effective WC-matrix interface cohesiveness during the prolonged cavitation exposure periods.
- The sub-surface damage morphology provides coherent input in terms of the ability of binder matrix to sustain the forces due the bubble implosion during cavitation.
- The particle velocity appears to play an important role in achieving a dense coating with an increased level of compressive stresses and gives rise to higher elastic strain energy during indentation.

Acknowledgments

The authors thankfully acknowledge the management of CPRI for according permission to publish this paper. The work carried out in the present study forms part of in-house Research Contingency project R-MTD-02 supported by CPRI. The support in the supply of HVAF coatings by Kermatico, USA and HVOF coating by M/s Spraymet surface technologies Pvt. Ltd, Bangalore, India is highly acknowledged.

References

1. J.F. Santa, L.A. Espitia, J.A. Blanco, S.A. Romo, and A. Toro, Slurry and Cavitation Erosion Resistance of Thermal Spray Coatings, *Wear*, 2009, **267**, p 160-167
2. M.K. Padhy and R.P. Saini, A Review on Silt Erosion in Hydro Turbines, *Renew. Sustain. Energy Rev.*, 2008, **12**, p 1974-1987
3. R.P. Singh, Silt Damage Control Measures for Underwater Parts: Nathpa Jhakri Hydro Power Station: Case Study of a Success Story, *Water Energy Int.*, 2009, **66**, p 36-42
4. R. Singh, S.K. Tiwari, and S.K. Mishra, Cavitation Erosion in Hydraulic Turbine Components and Mitigation by Coatings: Current Status and Future Needs, *J. Mater. Eng. Perform.*, 2012, **21**, p 1539-1551
5. B. Thapa, P. Chaudhary, O.G. Dahlhaug, and P. Upadhyay, Study of Combined Effect of Sand Erosion and Cavitation in Hydraulic Turbines, *Int. Conf. Small Hydropower*, 2007, **22**, p 24
6. K. Zhao, C. Gu, F. Shen, and B. Lou, Study on Mechanism of Combined Action of Abrasion and Cavitation Erosion on Some Engineering Steels, *Wear*, 1993, **162--164**, p 811-819
7. P.P. Gohil and R.P. Saini, Coalesced Effect of Cavitation and Silt Erosion in Hydro Turbines: A review, *Renew. Sustain. Energy Rev.*, 2014, **33**, p 280-289
8. L.M. Berger, S. Saaro, T. Naumann, M. Wiener, V. Weihnacht, S. Thiele, and J. Suchanek, Microstructure and Properties of HVOF-Sprayed Chromium Alloyed WC-Co and WC-Ni Coatings, *Surf. Coatings Technol.*, 2008, **2008**(202), p 4417-4421
9. S.J. Matthews, B.J. James, and M.M. Hyland, Microstructural Influence on Erosion Behavior of Thermal Spray Coatings, *Mater. Charact.*, 2007, **58**, p 59-64
10. M. Factor and I. Roman, Use of Microhardness as a Simple Means of Estimating Relative Wear Resistance of Carbide Thermal Spray Coatings: Part 2 Wear Resistance of Cemented Carbide Coatings, *J. Therm. Spray Technol.*, 2002, **11**(4), p 482-495
11. H. Li, K.A. Khor, and P. Cheang, Young's Modulus and Fracture Toughness Determination of High Velocity Oxy-Fuel-Sprayed Bioceramic Coatings, *Surf. Coat. Technol.*, 2002, **155**, p 21-32
12. L.-M. Berger, P. Ettmayer, P. Vuoristo, T. Mäntylä, and W. Kunert, Microstructure and Properties of WC-10% Co-4% Cr Spray Powders and Coatings: Part 1. Powder Characterization, *J. Therm. Spray Technol.*, 2001, **10**(2), p 311-325
13. S. Wirojanupatump, P.H. Shipway, and D.G. McCartney, The Influence of HVOF Powder Feedstock Characteristics on the Abrasive Wear Behavior of Cr_xC_y: NiCr Coatings, *Wear*, 2001, **249**, p 829-837
14. H.L.D.V. Lovelock, Powder/Processing/Structure Relationships in WC-Co Thermal Spray Coatings: A Review of the Published Literature, *J. Therm. Spray Technol.*, 1998, **7**(3), p 357-373
15. H.H. Tawfik and F. Zimmerman, Mathematical Modeling of the Gas and Powder Flow in HVOF Systems, *J. Therm. Spray Technol.*, 1997, **6**(3), p 345-352
16. S.L. Liu, X.P. Zheng, and G.Q. Geng, Influence of Nano-WC-12Co Powder Addition in WC-10Co-4Cr AC-HVAF Sprayed Coatings on Wear and Erosion Behaviour, *Wear*, 2010, **269**, p 362-367
17. G. Bolelli, L.-M. Berger, T. Börner, H. Koivuluoto, L. Lusvarghi, C. Lyphout et al., Tribology of HVOF- and HVAF-Sprayed WC–10Co4Cr Hard Metal Coatings: A Comparative Assessment, *Surf. Coatings Technol.*, 2015, **265**, p 125-144
18. C. Deng, M. Liu, C. Wu, K. Zhou, and J. Song, Impingement Resistance of HVAF WC-Based Coatings, *J. Therm. Spray Technol.*, 2007, **16**(5–6), p 604-609
19. Q. Wang, S. Zhang, Y. Cheng, J. Xiang, X. Zhao, and G. Yang, Wear and Corrosion Performance of WC-10Co4Cr Coatings Deposited by Different HVOF and HVAF Spraying Processes, *Surf. Coat. Technol.*, 2013, **218**, p 127-136
20. G. Bolelli, T. Börner, A. Milanti, L. Lusvarghi, J. Laurila, and H. Koivuluoto, Kari Niemi and Petri Vuoristo, Tribological behavior of HVOF- and HVAF-Sprayed Composite Coatings Based on Fe-Alloy+WC–12% Co, *Surf. Coat. Technol.*, 2014, **248**, p 104-112
21. L. Jacobs, M.M. Hyland, and M. De Bonte, Comparative Study of WC-Cermet Coatings Sprayed via the HVOF and the HVAF Process, *J. Therm. Spray Technol.*, 1998, **7**(2), p 213-218
22. T.C. Hanson and G.S. Settles, Particle Temperature and Velocity Effects on the Porosity and Oxidation of an HVOF Corrosion-Control Coating, *J. Therm. Spray Technol.*, 2003, **12**(3), p 403-415
23. M. Watanabe, A. Owada, S. Kuroda, and Y. Gotoh, Effect of WC Size on the Interface Fracture Toughness of WC-Co HVOF Sprayed Coatings, *Surf. Coat. Technol.*, 2006, **201**, p 619-627
24. P. Suresh Babu, B. Basu, and G. Sundararajan, Processing-Structure-Property Correlation and Decarburization Phenomenon in Detonation Sprayed WC-12Co Coatings, *Acta Mater.*, 2008, **56**, p 5012-5026

25. T. Varis, T. Suhonen, A. Ghabchi, A. Valarezo, S. Sampath, X. Liu, and S.P. Hannula, Formation Mechanisms, Structure, and Properties of HVOF-Sprayed WC-CoCr Coatings: An Approach Toward Process Maps, *J. Therm. Spray Technol.*, 2014, **23**(6), p 1009-1018
26. K. Niihara, A Fracture Mechanics Analysis of Indentation-Induced Palmqvist Cracks in Ceramics, *J. Mater. Sci. Lett.*, 1983, **2**, p 221-223
27. P.S. Prevey, Current Applications of X-ray Diffraction Residual Stress Measurement, *Dev. Mater. Charact. Technol*. G. Vander Voort and J. Friel (Eds.), 1996, p 103–110
28. J. Steller, International Cavitation Erosion Test and Quantitative Assessment of Material Resistance to Cavitation, *Wear*, 1999, **233--235**, p 51-64
29. R.K. Kumar, S. Seetharamu, and M. Kamaraj, Quantitative Evaluation of 3D Surface Roughness Parameters During Cavitation Exposure of 16Cr – 5Ni Hydro Turbine Steel, *Wear*, 2014, **320**, p 16-24
30. D.A. Stewart, P.H. Shipway, and D.G. McCartney, Microstructural Evolution in Thermally Sprayed WC-Co Coatings: Comparison Between Nanocomposite and Conventional Starting Powders, *Acta Mater.*, 2000, **48**, p 1593-1604
31. M.M. Lima, C. Godoy, J.C. Avelar-Batista, and P.J. Modenesi, Toughness Evaluation of HVOF WC-Co Coatings Using Nonlinear Regression An alysis, *Mater. Sci. Eng. A.*, 2003, **357**, p 337-345
32. Y.Y. Santana, P.O. Renault, M. Sebastiani, J.G. LA Barbera, J. Lesage, E. Bemporad et al., Characterization and Residual Stresses of WC-Co Thermally Sprayed Coatings, *Surf. Coat. Technol.*, 2008, **202**, p 4560-4565
33. P. Bansal, P.H. Shipway, S.B. Leen, and L.C. Driver, Experimental Validation of FE Predicted Fracture Behavior in Thermally Sprayed Coatings, *Mater. Sci. Eng. A.*, 2006, **430**, p 104-112
34. P. Bansal, P.H. Shipway, and S.B. Leen, Effect of Particle Impact on Residual Stress Development in HVOF Sprayed Coatings, *J. Therm. Spray Technol.*, 2006, **15**(4), p 570-575
35. R.K. Kumar, M. Kamaraj and S. Seetharamu, Cavitation Erosion Resistance Characteristics of HVOF and HVAF Processed 86WC-10Co4Cr Hydro Turbine Coatings, *Proc. 6th Asian Therm. Spray Conf. (ATSC-2014),* 2014, p 2–3
36. J. Nohava, B. Bonferroni, G. Bolelli, and L. Lusvarghi, Interesting Aspects of Indentation and Scratch Methods for Characterization of Thermally-Sprayed Coatings, *Surf. Coat. Technol.*, 2010, **205**, p 1127-1131